ARTICLE

CMIP is a negative regulator of T cell signaling

Julie Oniszczuk[1,2], Kelhia Sendeyo[1,2], Cerina Chhuon[3], Berkan Savas[1,2], Etienne Cogné[1,2], Pauline Vachin[1,2], Carole Henique[1,2], Ida Chiara Guerrera[3], Giuseppe Astarita[4], Vincent Frontera[1,2], Andre Pawlak[1,2], Vincent Audard[1,2,5,6], Dil Sahali[1,2,5,6] and Mario Ollero[1,2]

Upon their interaction with cognate antigen, T cells integrate different extracellular and intracellular signals involving basal and induced protein–protein interactions, as well as the binding of proteins to lipids, which can lead to either cell activation or inhibition. Here, we show that the selective T cell expression of CMIP, a new adapter protein, by targeted transgenesis drives T cells toward a naïve phenotype. We found that CMIP inhibits activation of the Src kinases Fyn and Lck after CD3/CD28 costimulation and the subsequent localization of Fyn and Lck to LRs. Video microscopy analysis showed that CMIP blocks the recruitment of LAT and the lipid raft marker cholera toxin B at the site of TCR engagement. Proteomic analysis identified several protein clusters differentially modulated by CMIP and, notably, Cofilin-1, which is inactivated in CMIP-expressing T cells. Moreover, transgenic T cells exhibited the downregulation of GM3 synthase, a key enzyme involved in the biosynthesis of gangliosides. These results suggest that CMIP negatively impacts proximal signaling and cytoskeletal rearrangement and defines a new mechanism for the negative regulation of T cells that could be a therapeutic target.

Keywords: CMIP; Transgenic mice; T cells

Cellular & Molecular Immunology (2020) 17:1026–1041; https://doi.org/10.1038/s41423-019-0266-5

INTRODUCTION

T cells play a central role in adaptive immunity through their close interplay with humoral and cellular sensors of innate immunity.[1] T cell activation is initiated by ligation of the TCR by an appropriate peptide bound to a major histocompatibility complex (MHC) molecule, which triggers rapid Src kinase-mediated phosphorylation of the immunoreceptor tyrosine-based activation motif (ITAM), a conserved domain of signal-transducing chains in the TCR complex.[2] Phosphorylated ITAMs serve as binding sites for ZAP-70 kinase, which is activated by its phosphorylation by the Src kinase Lck, stabilizing the ITAM-ZAP 70 interaction. Active TCRs are clustered, and the Src kinases Lck and Fyn and ZAP-70 are recruited in lipid rafts (LR), which are plasma membrane microdomains enriched in cholesterol and glycosphingolipids that serve as signaling platforms, in T cells.[3] Activation of ZAP-70 induces the phosphorylation of the transmembrane adapter molecule LAT (linker for activation of T cells) at multiple tyrosine residues and leukocyte phosphoprotein of 76 kDa (SLP-76), generating a signaling multicomplex within LRs through protein-protein or protein-lipid interactions. Activation of costimulatory molecules, such as CD28, promotes the recruitment of kinases and adapter proteins within LRs, which induces cytoskeletal reorganization that leads to the formation of immunological synapses. Immobilization of signaling molecules by cytoskeletal actin filaments and scaffold proteins may facilitate more efficient signal transmission from rafts to downstream signaling cascades, ultimately resulting in the activation of transcription factors, such as NF-kB, NFAT, and AP-1.[4]

CMIP (C-Maf-inducing protein) was initially identified in T cells from patients with minimal change nephrotic syndrome (MCNS), a renal disease of unknown immune origin.[5] The predicted structure of the 86-kDa natural isoform of CMIP includes an N-terminal region containing a pleckstrin homology domain (PH); a middle region characterized by the presence of several interacting docking sites, including a 14-3-3 module, a PKC domain, three potential ERK domains and an SH3 domain similar to the p85 regulatory subunit of phosphatidylinositol 3-kinase (PI3K); and a C-terminal region containing a leucin-rich repeat (LRR) domain.

CMIP has been found to be overexpressed in podocytes during INS relapse and in membranous nephropathy, another immune-mediated glomerular disease.[6,7] Recent studies showed that CMIP is also induced in some T cell subsets in patients with active systemic lupus erythematosus[8] and INS-like disease associated with cancers.[9,10] Increased CMIP abundance in these various pathological conditions may reflect different mechanisms of its induction that are possibly cell-specific. In fact, CMIP moves from the cytoplasm to the plasma membrane through its PH domain or to the nuclear compartment via its nuclear localization site, and this shuttling implies its interactions with different partners. For instance, several CMIP partners have been identified by the yeast two-hybrid system and confirmed by immunoprecipitation; these partners include the Src kinase Fyn, the P85 subunit of PI3 kinase,

[1]Institut National de la Santé et de la Recherche Médicale (INSERM), UMRS 955, Equipe 21, F-94010 Créteil, France; [2]Faculté de Médecine, Université Paris Est, UMRS 955, Equipe 21, F-94010 Créteil, France; [3]Proteomic Platform Necker, PPN-3P5, Structure Fédérative de Recherche SFR Necker US24, 75015 Paris, France; [4]Department of Biochemistry, Molecular and Cellular Biology, Georgetown University, Washington, DC, USA; [5]AP-HP, Groupe Henri-Mondor Albert-Chenevier, Service de Néphrologie, F-94010 Créteil, France and [6]Institut Francilien De Recherche En Néphrologie Et Transplantation, F-94010 Créteil, France
Correspondence: Dil Sahali (dil.sahali@inserm.fr)
These authors contributed equally: Julie Oniszczuk, Kelhia Sendeyo

Received: 1 December 2018 Accepted: 10 July 2019
Published online: 8 August 2019

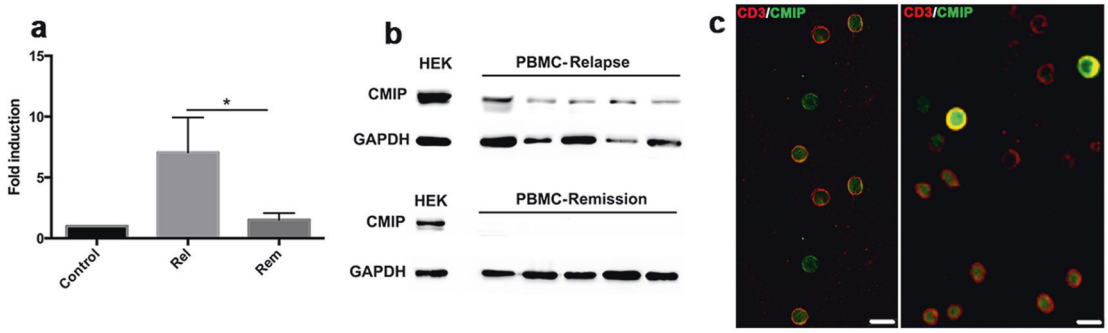

Fig. 1 Expression of CMIP in MCNS. **a** RT-qPCR to determine CMIP expression in healthy subjects ($n = 10$) and MCNS patients ($n = 10$) at relapse and in steroid-free remission. The data are quantified as the fold-change in induction relative to the control subject (mean with SEM, $^*p = 0.0156$, Mann-Whitney test). **b** Western blot analysis of CMIP expression in the PBMCs of MCNS patients in relapse and remission. HEK cells transfected with recombinant human CMIP served as a positive control. **c** Confocal microscopy analysis of Tcells isolated by negative immunoselection and double-labeled with CMIP (green) and CD3 (red) antibodies. Left panel: control: healthy subject; right panel: MCNS T cells from relapse

RelA (the p65 subunit of NF-kB), filamin A, and DIP-1 (death-associated protein kinase (DAPK)-interacting protein 1), among others.[11–13] By interacting with RelA, CMIP prevents RelA nuclear translocation and inhibits NF-kB activation.[11,14] In podocytes, CMIP promotes apoptosis by inducing caspase-3 activity, which upregulates the proapoptotic protein Bax and downregulates the antiapoptotic protein Bcl-2.[15] However, CMIP is scarcely detectable at both the transcript and protein levels in adult tissues under physiological conditions, which is due at least in part to its notable transcriptional repression by NF-kB and WT1, two master transcription factors.[16,17]

The increase in CMIP transcript levels in lymphocytes from patients with MCNS constitutes one of the hallmarks of MCNS relapse,[6] strongly suggesting the potential involvement of CMIP in disease pathogenesis and regulation of the immune response, but its precise role is currently unknown. Given that sequence analysis of CMIP coding regions shows a strong identity (99%) between CMIP in humans, mice and rats, we generated transgenic mice selectively overexpressing CMIP in mature lymphocytes. In the present study, we aimed to understand the role of CMIP in T cell signaling by thoroughly observing the impact of its overexpression on the T cell response.

RESULTS

Expression of CMIP in human T cells

We first analyzed the expression of CMIP at the mRNA and protein levels in patients with MCNS relapse and remission, as well as in control healthy subjects. Expression of the transcript was measured by real-time quantitative PCR (RT-qPCR), with each patient analyzed in relapse and steroid-free remission ($n = 10$). The transcript levels in patients were quantified as fold-changes in induction relative to transcript levels in control subjects. We found MCNS relapse to be associated with a significant increase in CMIP abundance (Fig. 1a). Western blots of PBMC lysates showed a slight band recognized by polyclonal CMIP antibody at the expected size in patients with MCNS relapse (Fig. 1b), but this band was scarcely detected or absent in patients in remission. Immunofluorescence analysis indicated that CMIP was expressed selectively in a subset of T cells (Fig. 1c), but the unavailability of CMIP-specific monoclonal antibodies precluded accurate characterization of this subset by flow cytometry.

Generation of CMIP transgenic mice

To analyze the functional consequences of CMIP overexpression in vivo, we used a targeting system in which a construct containing a single copy of the human CMIP coding sequence downstream of the Lck distal promoter was inserted into the X-linked hypoxanthine phosphoribosyltransferase (Hprt) locus by homologous recombination (Fig. 2a). It has been established that the Lck distal promoter drives transgene expression in peripheral T cells.[18] We obtained six founders, which were crossed with wild-type (WT) BALB/c mice and backcrossed repeatedly to obtain a homogeneous BALB/c genetic background. Because the transgene is expressed in the X chromosome, all mice analyzed within the current study were hemizygous males, which was confirmed by tail genotyping, from the F10 to F18 generations (Fig. 2b). Transgene expression was demonstrated at the transcriptional level in splenic T cells (Fig. 2c). Although the endogenous CMIP transcript was detected in WT (control littermates) splenic T cells, immunofluorescence labeling using two different polyclonal antibodies detected a significant signal for the CMIP transcript in transgenic mice, but this signal was scarce in WT splenic T cells (Fig. 2d). Examination of the thymus, node and spleen during follow-up showed that the basal phenotype of transgenic mice was normal, and no lymphoproliferative syndrome was observed until one year of age.

CMIP transgenic mice exhibit a "naïve" T cell phenotype

To assess the influence of CMIP expression on T cell compartments, we determined the frequencies of the main peripheral T cell subsets by FACS analysis. Splenocytes from 12-week-old mice were purified and stained with antibodies against CD4, CD8, CD44, and CD62L. Although the number of CD3 T cells and the percentages of either $CD4^+$ or $CD8^+$ T cells were comparable between WT and transgenic mice ($n = 5$ mice in each group) (Fig. 3a, b), the frequencies of naïve $CD4^+$ T cells ($CD4^+CD44^{low}CD62L^{high}$) and naïve $CD8^+$ T cells ($CD8^+CD44^{low}CD62L^{high}$) were significantly increased in Tg mice, whereas the frequencies of memory and effector T cells ($CD44^{high}CD62L^{high}$ and $CD44^{high}CD62L^{low}$, respectively) were decreased in both Tg $CD4^+$ and $CD8^+$ T cells (Fig. 3c, d). We next analyzed T cell proliferative ability following CD3/CD28 stimulation. T cells were cultured ex vivo in quiescent conditions (6 h in the presence of 2% FCS) and then incubated in complete medium containing 10% FCS in the presence of anti-CD3/CD28 antibodies (1 µg/ml each). After staining with CFSE at day 0, T cells were allowed to proliferate for 5 days and then analyzed by flow cytometry. As attested by CFSE dilution, the percentage of dividing cells was lower in transgenic T cells than in WT T cells, but the addition of IL-2 to the culture medium restored the proliferative capacity of transgenic T cells to control levels (Fig. 3e, S1).

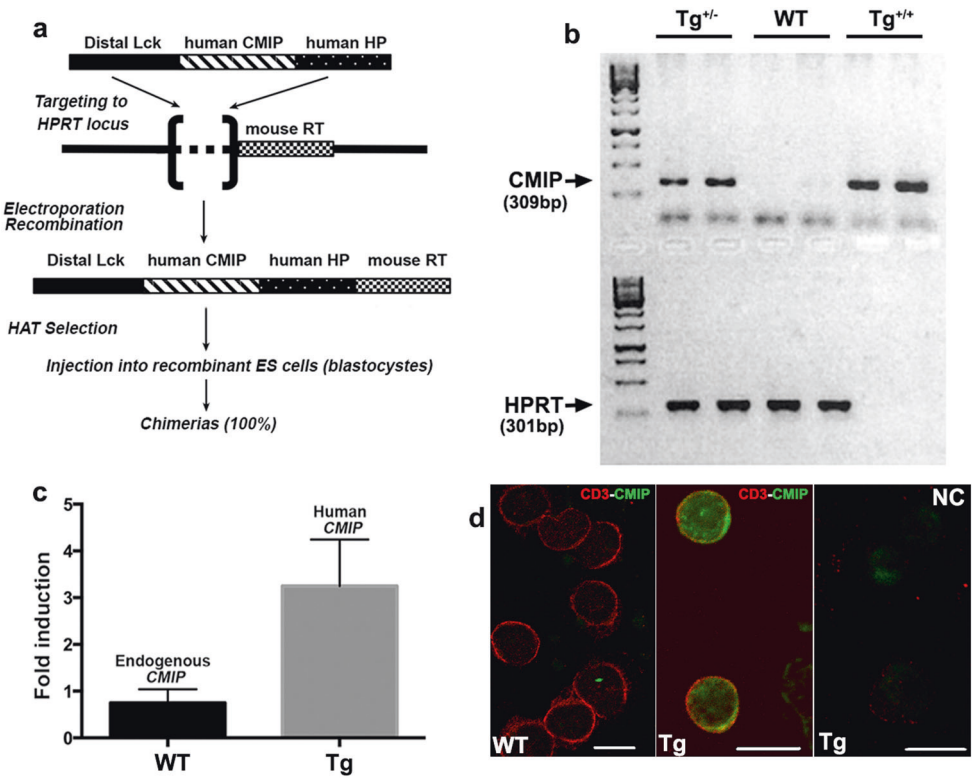

Fig. 2 Generation of CMIP transgenic mice. **a** Schematic diagram of targeted transgenesis into the HPRT locus (see details in the Materials and Methods section). All mice analyzed in this study were hemizygous males from the F10 to F18 generations. **b** PCR genotyping of mouse tail DNA. The HPRT PCR product was amplified from the WT allele in homozygous transgenic females (Tg+/+) or hemizygous transgenic males (Tg+) but not the reconstituted HPRT gene. **c** Quantification of mouse and human CMIP transcripts in transgenic mice and WT mice by RT-qPCR. **d** Confocal immunofluorescence microscopy of CMIP expression in T cells from WT and transgenic mice. The rightmost figure in the panel corresponds to the negative control, in which IgG isotype control antibody was used instead of primary antibody (Cmip/CD4) in Tg T cells

Transgenic T cells display an impaired response to CD3-CD28 stimulation

We sought to determine the effects of the in vivo overexpression of CMIP on T cell activation and polarization. We first studied CMIP transgene expression in T cells isolated by negative immunoselection under resting and stimulating conditions. T cells were starved in RPMI medium containing 2% FCS for 6 h at 37 °C and then activated with anti-CD3/CD28 antibodies (1 µg/ml each). The abundance of the endogenous CMIP transcript quantified by RT-qPCR rapidly fell upon CD3/CD28 stimulation, and the endogenous protein was scarcely detected by Western blotting (Fig. 4a, b). In contrast, CMIP transgene expression driven by the Lck distal promoter was significantly increased at the mRNA and protein levels at early stages and peaked 1 h after activation (Fig. 4a, b). In physiological conditions, T cell activation is associated with the strong induction of NF-kB activity. Previous reports have shown that NF-kB is a repressor of CMIP transcriptional activation,[11,14] which may account for the downregulation of endogenous Cmip in WT mice.

We next analyzed whether expression of the CMIP transgene is associated with a particular pattern of cytokine production in T cells isolated by negative immunoselection. Because transgene abundance started to decline beginning 2 h after activation, we analyzed cytokine expression over the 16 h following CD3/CD28 activation by RT-qPCR, except for IL2 expression, as IL2 transcription started earlier after T cell stimulation. Compared with T cells from WT mice, T cells from transgenic mice exhibited significantly lower levels of IL-2, IL-4, and IFNγ, whereas the IL-10 level was increased (Fig. 4c). To assess whether cytokine production is affected by signals bypassing TCR stimulation, T cells were isolated by negative immunoselection and challenged with phorbol myristate ester (PMA, 50 ng/ml) and ionomycin (0.5 µg/ml). While decreased IL-2 production was found in Tg T cells stimulated by CD3/CD28, no significant difference between WT and Tg T cells following PMA/ionomycin activation was observed (Fig. S2). In contrast, increased levels of IL-4 and IFNγ transcripts were detected in WT T cells after 4 h of PMA/ionomycin activation, although the differences between IL-4 and IFNγ levels were less pronounced than those between TCR signals. Notably, the increased abundance of IL-10 mRNA in Tg T cells after CD3/CD28 stimulation was not found with PMA/ionomycin activation, which suggests that proximal signals arising from Tg T cells are required for IL-10 synthesis. Altogether, these results suggest that increased Cmip abundance is mainly associated with the inhibition of T cell activation and the differentiation of T cells into effector T cells.

CMIP expression is associated with the inactivation of Src kinases

In physiological situations, T cell activation results in a series of phosphorylation cascades that ultimately result in cellular proliferation, differentiation and cytokine production. The decreased reactivity of transgenic T cells in response to CD3-CD28 stimulation compared to that of WT T cells led us to investigate whether transgenic T cells are defective in the phosphorylation of some components that play a key role in early signaling. T cells were synchronized (6 h in the presence of 2% FCS) and then stimulated with anti-CD3/CD28 antibodies. Total protein lysates were collected at 1 h after activation and analyzed by Western blotting using the anti-phosphotyrosine monoclonal antibody 4G10. Wild-type T cells exhibited

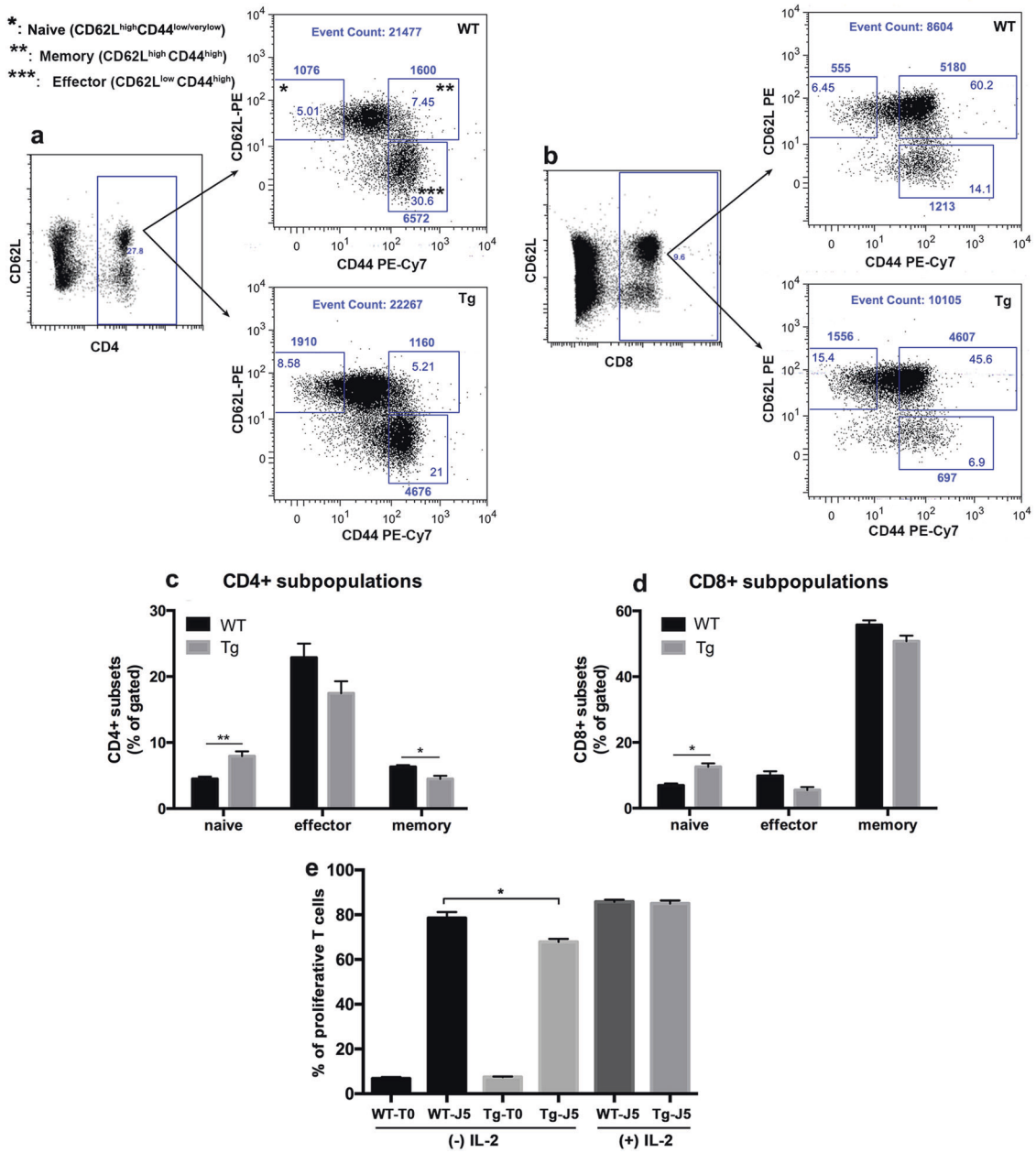

Fig. 3 Transgenic mice develop an altered T cell phenotype. **a**, **b** Representative flow cytometry analysis of naïve, effector and memory T cells in transgenic and WT T cells. Splenocytes from 12-week-old transgenic mice (Tg) and WT mice were gated for CD4 + cells (**a**) or CD8 + cells (**b**) and analyzed for CD44 and CD62L expression. T cell subpopulations were defined as naïve ($CD44^{low/verylow}CD62L^{high}$), memory ($CD44^{high}CD62L^{high}$), or effector T cells ($CD44^{high}CD62L^{low}$). The numbers inside and outside each small square indicate the percentage and the absolute number of cells, respectively. The total number of events is shown at the top. **c** and **d** Frequencies of naïve, effector and memory T cells. The results are representative of three independent experiments ($n = 5$ each for WT and transgenic mice). The frequency of naïve T cells in both CD4 + and CD8 + compartments was significantly increased, whereas the level of memory CD4 + T cells was decreased in transgenic mice compared to WT mice (Tg vs. WT, mean with SEM: naïve CD4 +, $^{**}p = 0.0079$; naïve CD8 +, $p = 0.0159$; memory CD4 +, $p = 0.0303$, Mann-Whitney test). Although effector CD4+ and CD8 + subsets were decreased in Tg mice, this difference did not reach statistical significance. **e** Transgenic T cells exhibited a decreased proliferative capacity compared to WT T cells. T cells were isolated from Tg and WT mice and labeled with CFSE (1 μM). After synchronization, the cells were stimulated with anti-CD3/CD28 antibodies (1 μg/ml each). After 5 days, proliferation was analyzed by flow cytometry as the percentage of dividing cells. The addition of mouse recombinant IL2 (30 U/ml) at 24 and 72 h after stimulation restored the T cell proliferation rate, which was comparable between Tg and WT mice. Data are presented as the mean of four independent experiments. (Tg vs. WT at day 5, mean with SD: * $p = 0.0286$, Mann-Whitney test)

substantial phosphorylation within a region spanning 60-70 kDa that was barely detected in Tg T cells (Fig. 5a). This region includes members of the Src kinase family, which are involved in the early steps of T cell activation, among others.[19] The Src kinase family comprises nine members, of which Lck and Fyn are the most abundant in T cells, that play a crucial role in the immune response.[20] Therefore, we tested the reactivity of protein lysates with an anti-Src antibody that recognizes the phosphotyrosine (pY) site at residue 418, which is specific to active Src kinases. A decrease in pY^{418}Src in transgenic T cells culminating 15 min after activation, which coincided with the highest levels of pY^{418}Src in WT T cells, was clearly observed

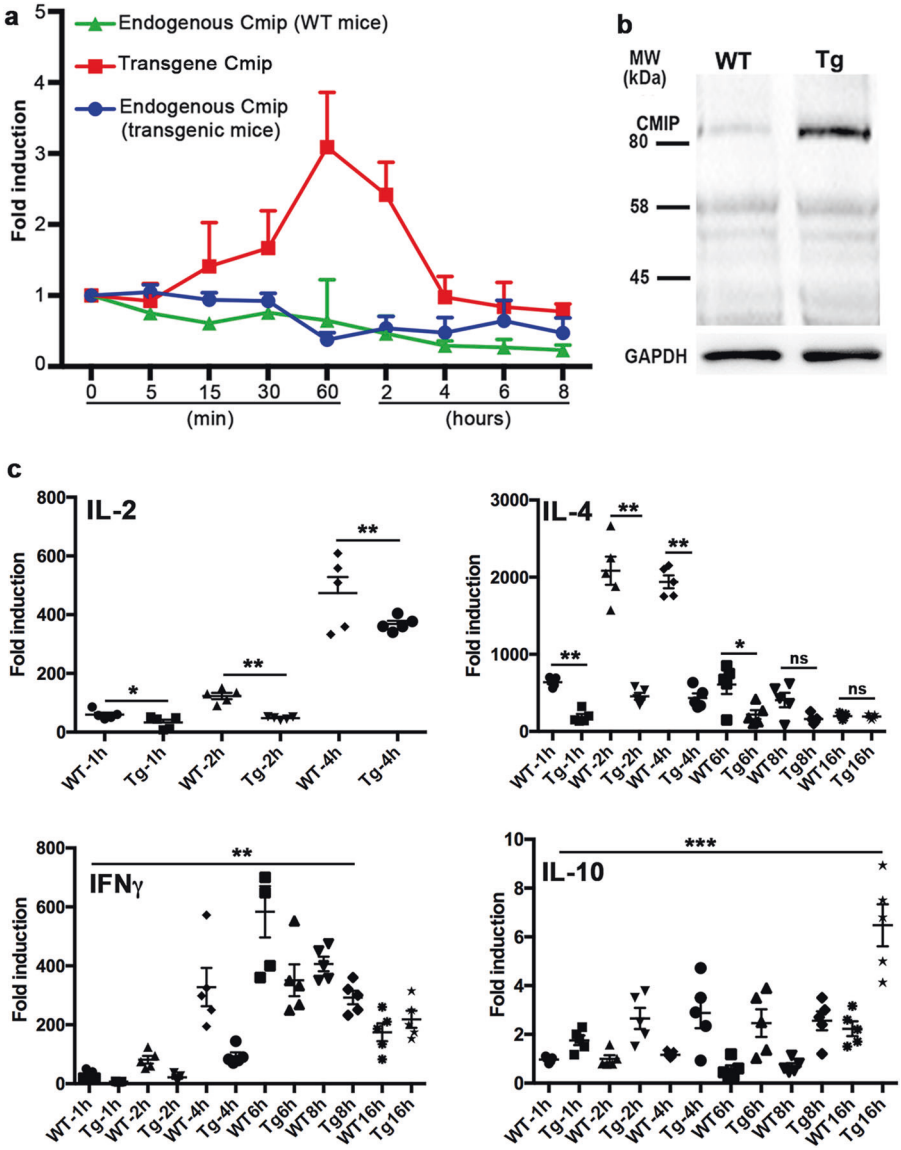

Fig. 4 Influence of CMIP induction on cytokine expression. **a** Expression of the CMIP transcript. Total RNA was extracted from synchronized T cells before and after CD3/CD28 stimulation (1 μg/ml each) at the indicated times. The expression of endogenous Cmip in WT (green) and Tg mice (blue) along with Tg Cmip (red) is shown. **b** Expression of CMIP protein under the same conditions. **c** IL-2, IFNγ, IL-4, and IL-10 transcripts were quantified by RT-qPCR. The results are representative of three independent experiments ($n = 5$ mice in each group). [Tg vs. WT, mean with SEM; IL-2, 1 h: $*p = 0.0278$, 2 h: $**p = 0.0040$, 4 h: $**p = 0.0040$; IL-4, 1 h: $**p = 0.0040$, 2 h: $**p = 0{,}0040$, 4 h: $**p = 0{,}0040$, 6 h: $*p = 0.0278$, 8 and 16 h: nonsignificant (ns); IFNγ, 1 h: $*p = 0.0257$, 2 h: $**p = 0.0040$, 4 h: $**p = 0.0079$, 6 h: $*p = 0.0317$, 8 h: $*p = 0.0317$ and 16 h: $p = 0.532$ (ns); IL-10, 1 h: $*p = 0.0286$, 2 h: $*p = 0.0159$, 4 h: $p = 0.1508$ (ns), 6 h: $*p = 0.0159$, 8 h: $**p = 0.0079$, 16 h: $**p = 0.0079$; Mann-Whitney tests]

(Fig. 5b). The early events of T cell activation involve the clustering of T cell receptors and costimulator molecules and recruitment of the Src kinases Fyn and Lck into LRs.[3] Lck phosphorylates ITAM motifs at intracellular CD3 domains and induces ZAP70 recruitment.[21] We evaluated the levels of pY^{505}Lck and pY^{528}Fyn, which are specific to the inactive forms of Lck and Fyn, respectively, after T cell stimulation. The abundance of pY^{505}Lck and pY^{528}Fyn was increased in transgenic T cells at baseline compare to that in WT T cells, which persisted after CD3/CD28 stimulation (Fig. 5c, d). We examined the phosphorylation levels of ZAP70 and observed a remarkable increase in the active form of ZAP70 (pY^{319}Zap 70) in WT T cells upon their stimulation but not in transgenic T cells (Fig. 5e). Interestingly, immunofluorescence analysis showed that pY^{418}Src was confined to a clustered compartment within the thin layer of subplasma membrane at 30 and 60 min after activation in WT T cells; this formation was not detected in Tg T cells (Fig. 5f). Overall, these results suggest that CMIP inhibits the first steps of T cell activation. This possibility was further assessed in Cmip-deficient T cells from a new mouse model of selective and doxycycline-inducible *CMIP* ablation in T cells (CD2-rtTA/TetOn-Cre/$CMIP^{loxP/loxP}$). Naïve CD4 T cells were purified from KO and control littermates (without doxycycline treatment) and stimulated by anti-CD3/CD28 antibodies (1 μg/ml each) for 15 and 30 min (Fig. S3). The levels of the inactive forms of the Src kinases Fyn and Lck was lower in Cmip-deficient T cells than in T cells from controls, whereas the abundance of active pY^{418} Src kinases and pY^{319}Zap70 was increased (Fig. S3,a-d). Genotyping and Western blotting confirmed that Cmip was expressed in control littermates and deleted in KO mice (Fig. S3,e).

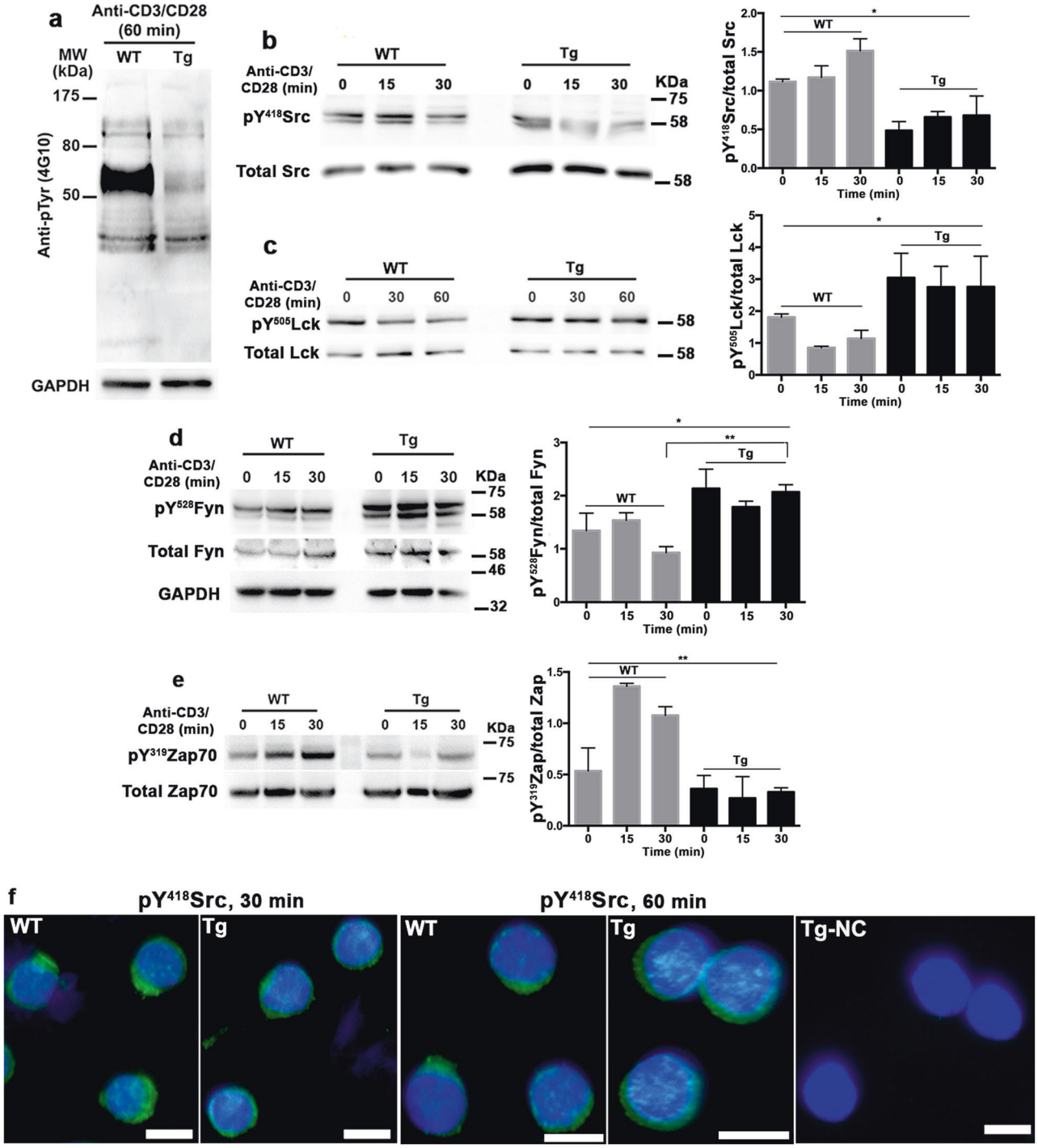

Fig. 5 Transgenic T cells exhibit a hypophosphorylated protein profile with the downregulation of active Src. **a** Representative Western blot of protein lysates from transgenic and WT T cells after 60 min of activation by anti-CD3/CD28 antibodies incubated with anti-phosphotyrosine 4G10; blots were stripped and reprobed with anti-GAPDH antibody. **b**–**e** Western blots of protein lysates from transgenic and WT T cells several time points following anti-CD3/CD28 antibody activation (1 μg/ml each); blots were stripped and reprobed with an antibody raised against total specific protein. The results are representative of three independent experiments [pY^{418}Src/total Src: one-way ANOVA, $^{*}p = 0.0163$; pY^{505}Lck/total Lck: Kruskal-Wallis test, $^{*}p = 0.0362$; pY^{528}Fyn/total GAPDH, one-way ANOVA, $^{*}p = 0.0204$, Tg vs. WT (30 min), $^{**}p = 0.0015$; pYr^{319}Zap70/total Zap70, one-way Anova, $^{**}p = 0.0068$]. **f** Immunofluorescence staining for pY^{418}Src in transgenic and WT T cells isolated by negative immunoselection

Transgenic T cells show the accumulation of inactive Fyn and Lck in LR

We investigated whether the clustering of LRs is compromised as a result of impaired Src kinase activation in transgenic T cells. We purified LRs at rest and 30 min following activation by anti-CD3/CD28 antibodies (1 μg/ml each) with a detergent-free OptiPrep method. Then, we tested the distribution of flotillin-1 and cholesterol by Western blotting and thin layer chromatography (TLC) and found them to be enriched in LR fractions. The observed difference in flotillin-1 and cholesterol signals between WT and Tg

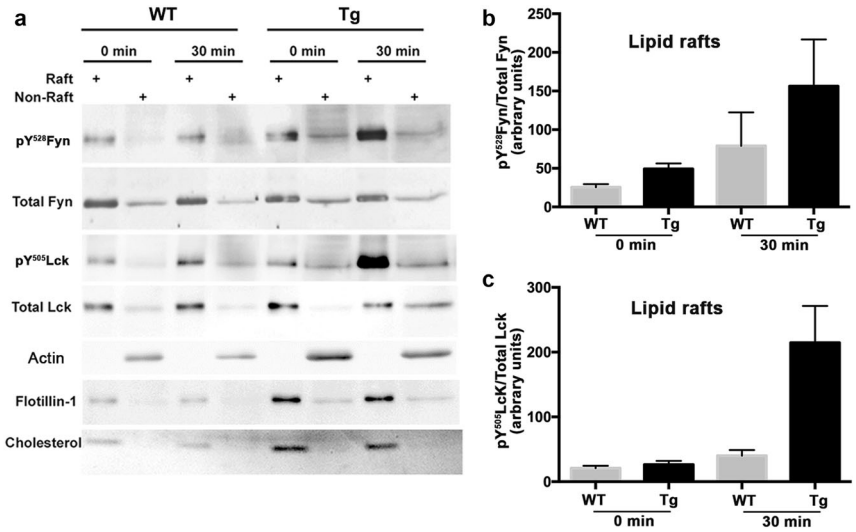

Fig. 6 Transgenic T cells exhibit higher levels of inactive Fyn and Lck in LRs and fail to be activated after CD3/CD28 costimulation. **a** Western blotting and TLC of raft (R) and nonraft (NR) fractions prepared at rest (0 min) and after the activation (30 min) of transgenic and WT mouse T cells. Rafts are enriched in Flotillin-1 and cholesterol. Samples were analyzed with anti-pY^{528}Fyn and anti-pY^{505}Lck antibodies, which recognize the inactive forms of Fyn and Lck, respectively, followed by antibodies recognizing total Fyn and Lck, respectively. Cholesterol was analyzed by TLC. **b**, **c** Inactive/total Fyn and inactive/total Lck in raft microdomains according to densitometric analysis of the bands shown in **a**

LRs was due to a difference in the input (Fig. 6a). Total Fyn and Lck were both found to be mostly localized to LRs at similar proportions, except in transgenic T cells, in which the total Lck was reduced in LRs after 30 min of activation. In resting conditions, the relative abundance of pY^{528}Fyn (inactive form) in LRs was twice as high in transgenic T cells than in WT T cells (Fig. 6a, b). The relative abundance of pY^{528}Fyn was dramatically increased in activated transgenic T cells, whereas it remained low in activated WT T cells. Although we found no difference in pY^{505}Lck abundance between transgenic and WT T cells in resting conditions, pY^{505}Lck was significantly increased in the LRs of activated transgenic T cells compared to that in WT T cells (Fig. 6a, c). These results suggest that the decreased reactivity of transgenic T cells compared to that of WT T cells results from the inactivation of Src kinases in LRs linked to the CMIP-mediated inhibition of proximal signaling.

Transgenic T cells fail to polarize during CD3/CD28 costimulation
T cell polarization after CD3/CD28 stimulation involves the migration and aggregation of lipid raft microdomains at the site of immunological synapse formation.[22] We evaluated whether the distribution of LRs in transgenic T cells was affected using the lipid raft marker cholera toxin B (CTB), which preferentially binds the ganglioside M1 (GM1) glycosphingolipid. We performed double fluorescence labeling with anti-Src antibody and CTB. WT T cells exhibited the polarized colocalization of both markers 30 min after activation (Fig. 7a). However, we did not detect any polarization in transgenic T cells, suggesting that CMIP interferes with LR migration. Then, we analyzed linker for activation of T cells (LAT), an adapter protein recruited at the plasma membrane that segregates into LRs upon engagement of the T cell receptor and costimulatory signaling. The membrane localization and distributions of LAT and CTB (coupled with Alexa Fluor 555) were examined by fluorescence staining 30 min after T cell activation by anti-CD3/CD28 antibodies (1 µg/ml each). While LAT and CTB were clustered in plasma membrane microdomains in WT T cells, they were spread along the plasma membrane in transgenic T cells (Fig. 7b). We next monitored LR dynamics following anti-CD3/CD28 antibody costimulation. T cells from transgenic and WT mice were isolated by negative immunoselection, stained with AF555-CTB, and then incubated in the presence of anti-CD3-coated beads and soluble anti-CD28 (1 µg/ml). The time-dependent distribution of fluorescence was evaluated by video microscopy. CTB moved from the periphery and formed a cluster at the contact points between T cells and anti-CD3-coated beads (Fig. 8d and Movie S1). Conversely, CTB did not move toward anti-CD3-coated beads in transgenic T cells, suggesting that the beads were unable to reorganize GM1-positive microdomains. Collectively, these results suggest that CMIP prevents LR clustering required for the formation of immunological synapses and effective T cell activation.

CMIP alters glyco/gangliosphingolipid metabolism
To examine whether CMIP overexpression modifies the dynamics and lipid composition of cell membranes, we used mouse podocytes from an immortalized independent cell line that were stably transfected with the CMIP coding sequence optimized for untargeted global lipidomics analysis. Principal component analysis (PCA) of our lipidomic data showed the clear clustering of our samples into two groups that discriminated between CMIP-transfected and empty vector-transfected control cells (EV). Figure 8a shows PCA in which both positive and negative ions had been combined. The lipids that contributed most to the variance between groups were isolated using ANOVA ($p < 0.001$ and fold-change > 5). Pathway topology analysis of KEGG pathways using Metabolomics Pathway Analysis (MetPA) showed that CMIP expression had a strong impact on sphingolipid metabolism (Fig. 8b). In addition, independent overrepresentation analysis across multiple pathways sources using IMPaLa confirmed that the most significant alteration in CMIP expression affected glyco/gangliosphingolipid metabolism (Data file S1). Consistently, the levels of GM3 and GM2 species were significantly decreased, whereas the levels of GM1 species increased in CMIP-expressing cells compared to those in control cells (Fig. 8c). To understand the mechanism leading to these modifications to the ganglioside profile, we used Western blotting to evaluate the expression level of GM3 synthase, a key enzyme in the biosynthesis of ganglio-series gangliosides responsible for the conversion of LacCer into GM3. We observed the decreased expression of GM3 synthase in Tg cells compared to that in WT cells, especially at 30 and 60 min after activation (Fig. 8d). This result suggests that a decrease in GM3 synthase expression contributes, at least in part, to the

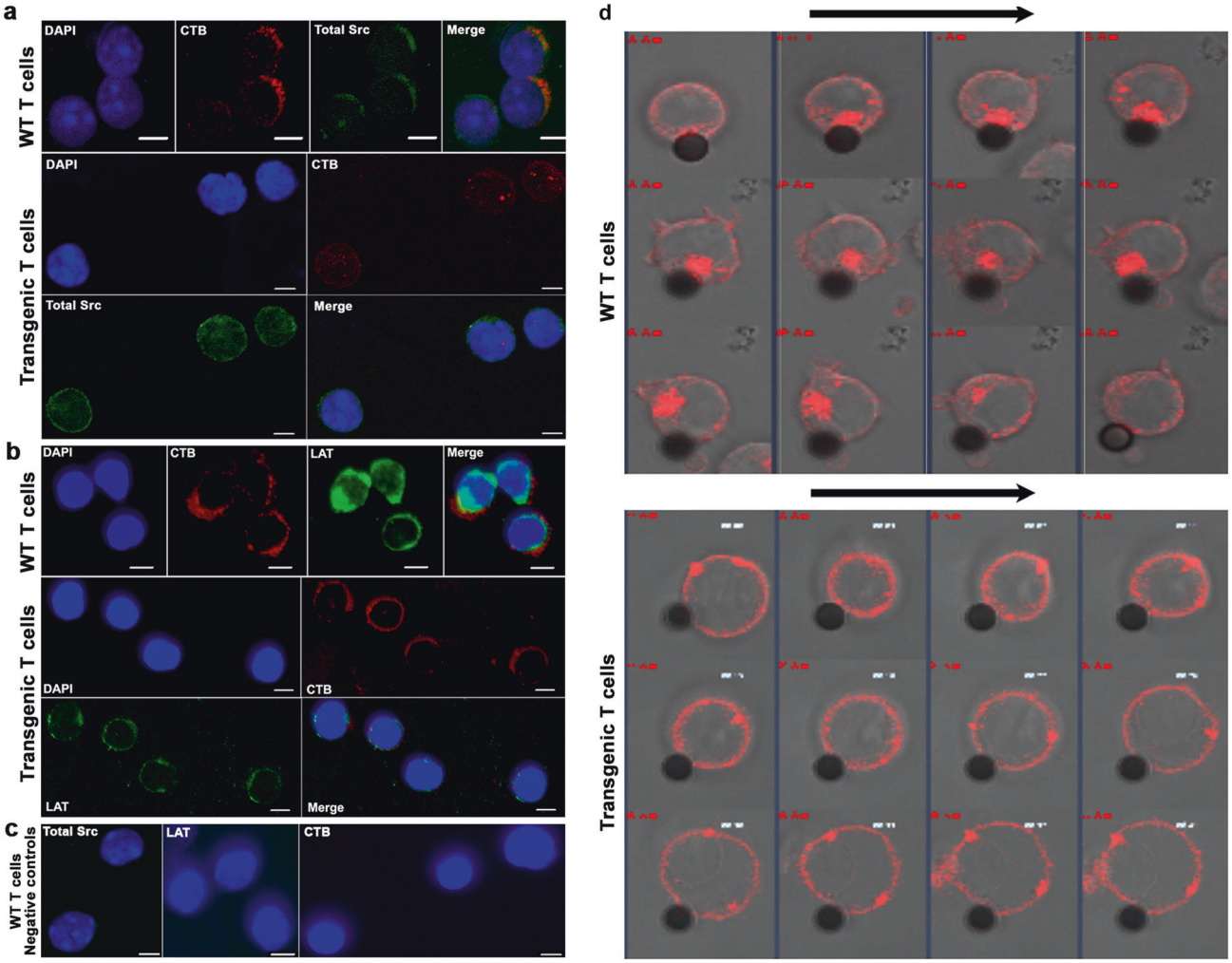

Fig. 7 CMIP inhibits clustering and activation of the raft signaling platform. **a** CMIP inhibits membrane clustering of Src kinases and CTB after CD3/CD28 stimulation. Immunofluorescence analysis of transgenic and WT T cells after 30 min of activation by anti-CD3/CD28 antibodies (1 μg/ml each) that were then fixed and immunostained for total Src (green) and CTB (red). Cellular nuclei were revealed by counterstaining with DAPI dye. Confocal analysis shows that Src kinases and CTB colocalize in WT but not transgenic T cells. **b** CMIP inhibits the clustering of LAT and CTB into LRs after CD3/CD28 stimulation. Fluorescence analysis of LAT and CTB after T cell activation performed as in **a**. **c** Negative Src, LAT and CTB controls: the specificity of each signal in WT T cells was assessed using IgG isotype control antibody instead of primary antibody. **d** CMIP inhibits LR clustering and T cell polarization. Transgenic and WT T cells were synchronized, stained with CTB, loaded into 8-well plates at 50,000 cells/well and activated with anti-CD3-coated beads (cells:beads, 2:1) and soluble anti-CD28 (1 μg/ml). Cells were kept at 37 °C. Data were acquired with a confocal microscope at 1 image/15 s. Images were extracted from movies (1 image/min) and analyzed by ImageJ software (magnification: ×63)

downregulation of GM3 and GM2 observed in cells overexpressing CMIP.

Proteomic analysis of T cells isolated from WT and transgenic mice
To further evaluate the impact of CMIP expression on T cell signaling, we performed differential proteomic analysis of T cells from 12-week-old transgenic and WT mice (twelfth generation, $n = 3$ each). T cells were purified by negative immunoselection and then activated by anti-CD3/CD28 antibodies (1 μg/ml each). At 0 and 60 min after stimulation (corresponding to the time of highest transgene expression), total proteins were extracted and digested with trypsin, and the peptides in three parallel technical replicates per sample were quantified. The expression levels of the 2660 identified proteins in four conditions were compared (Data file S2). As a result, 46 proteins were found to be differentially expressed between transgenic and WT T cells as a function of T cell activation (two-way ANOVA interaction, $p < 0.05$) (Data file S3). Hierarchical clustering displayed four major clusters grouping proteins whose expression varied in the different experimental conditions (Fig. 9a, Table 1). Under basal conditions, a cluster of 9 proteins (cluster 1) were found to be highly expressed in WT T cells, while they were strongly downregulated in transgenic T cells. This cluster includes two proteins involved in lipid remodeling, namely, HRAS-like suppressor 3 (Pla2g16) and ethanolamine phosphate cytidylyltransferase (Pcyt2). In activated T cells, the expression levels of a cluster of 13 proteins (cluster 2) were found to be depleted in WT mice but increased or unchanged in transgenic mice. This cluster includes proteins involved in the organization of the actin cytoskeleton, such as cofilin-1 (Cfl1), and nucleotide metabolism, such as creatine kinase B-type (Ckb), nicotinamide phosphoribosyltransferase (Nampt) and guanylate kinase (Guk1). Cluster 3 encompassed 10 proteins that were significantly downregulated in WT T cells relative to their expression in transgenic T cells in basal conditions. This cluster includes two proteins involved in lipid uptake and metabolism, namely, cell cycle control protein 50 A (Tmeme30a)

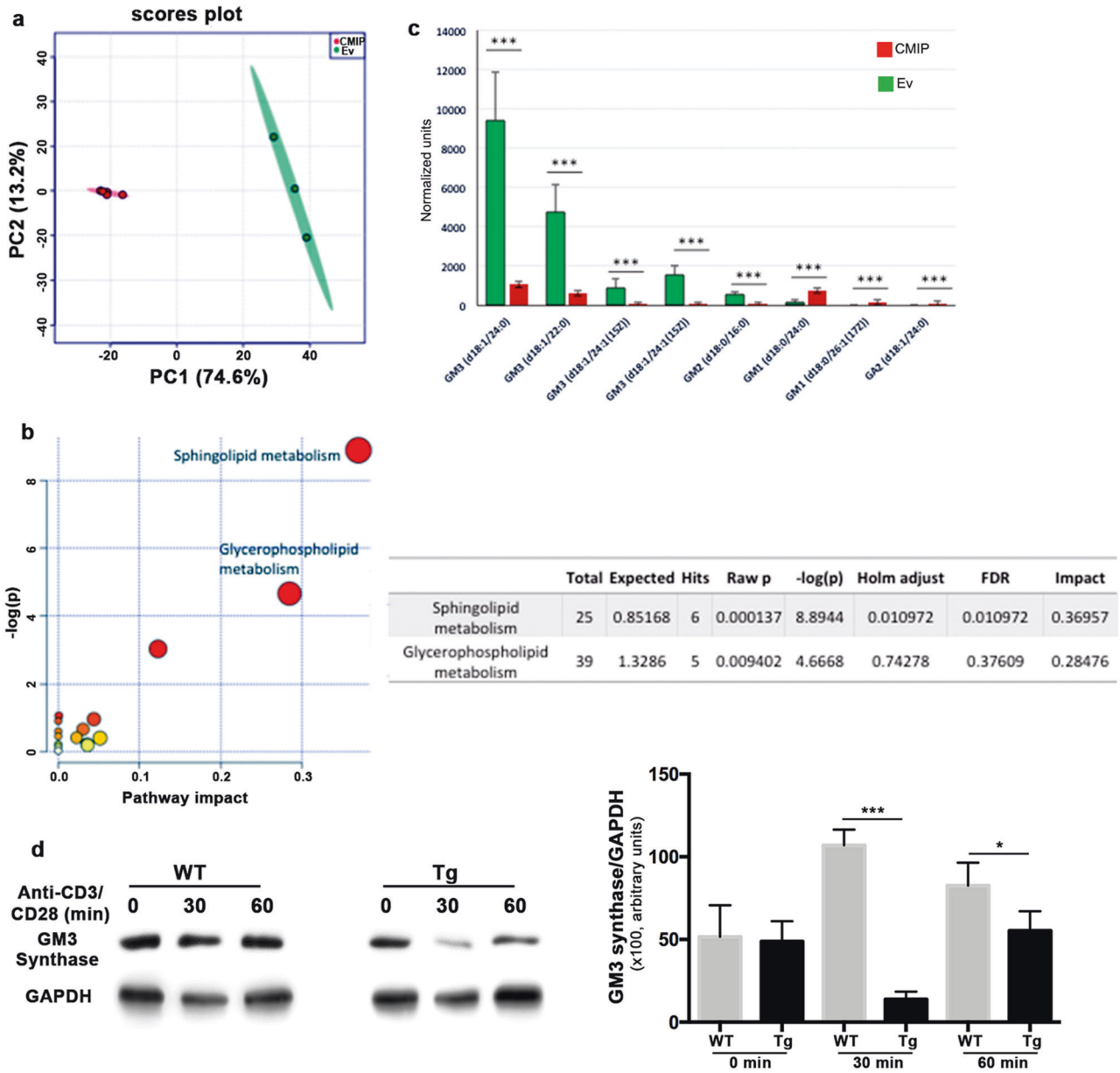

	Total	Expected	Hits	Raw p	-log(p)	Holm adjust	FDR	Impact
Sphingolipid metabolism	25	0.85168	6	0.000137	8.8944	0.010972	0.010972	0.36957
Glycerophospholipid metabolism	39	1.3286	5	0.009402	4.6668	0.74278	0.37609	0.28476

Fig. 8 CMIP induces alterations in the glycosphingolipid biosynthetic pathway and ganglioside species. A mouse podocyte cell line was stably transfected with a CMIP expression vector or an empty vector (EV). Lipids were extracted and subjected to LC-MS analysis. **a** Principal component analysis of ion abundance in the positive and negative modes discriminated between CMIP-transfected and EV-transfected cells. PC1 accounted for 74.6% of the total variance. **b** Metabolome view after MetPA shows sphingolipid metabolism to be the pathway most significantly altered by CMIP expression. Total: the total number of compounds in the pathway; Hits: the actual matched number from the uploaded data; Raw p: original *p* value calculated from enrichment analysis; Holm p: p value adjusted by the Holm-Bonferroni method; FDR p: *p* value adjusted using the false discovery rate; Impact: pathway impact value calculated from pathway topology analysis. **c** The relative abundances of several ganglioside species are very significantly different between empty vector-transfected and CMIP-transfected cells. Data are expressed as the means ± SDs of normalized arbitrary units. ***$p < 0.001$. EV: $n = 3$. CMIP: $n = 6$. **d** Representative Western blot showing GM3 synthase (*St3Gal5* gene) in protein lysates at rest (0 min) or after 30 and 60 min of the activation of transgenic and WT T cells with anti-CD3/CD28 antibodies; blots were stripped and reprobed with anti-GAPDH antibody. Statistical analyses of three independent experiments were performed [Tg vs. WT (30 min), ***$p = 0.0005$ and Tg vs. WT (60 min), *$p = 0.0254$)]

and monoacylglycerol lipase (Abhd6). Most remarkably, a fourth cluster (cluster 4) comprised 14 proteins that underwent a dramatic increase in expression after stimulation in WT cells but were depleted in transgenic T cells under the same conditions. The most notable representative members of this cluster were inhibitor of nuclear factor kappa-B kinase subunit epsilon (Ikbke), casein kinase II subunit alpha (Csnk2a2), the cPLA2 inhibitor annexin-1 (Anxa1), and the lipid remodeling factor lysophosphatidic acid phosphatase 6 (Acp6). These results, along with other data obtained from the transgenic mouse model, suggest a defect in T cell activation associated with CMIP expression. Based on these findings, we further analyzed the expression of Cofilin-1, a major actor in the dynamic rearrangement of the actin cytoskeleton[23] whose activity was recently reported to be negatively regulated by CMIP in podocytes,[24] by Western blotting. We found that phosphorylated Cofilin-1, the inactive form of Cofilin-1, was

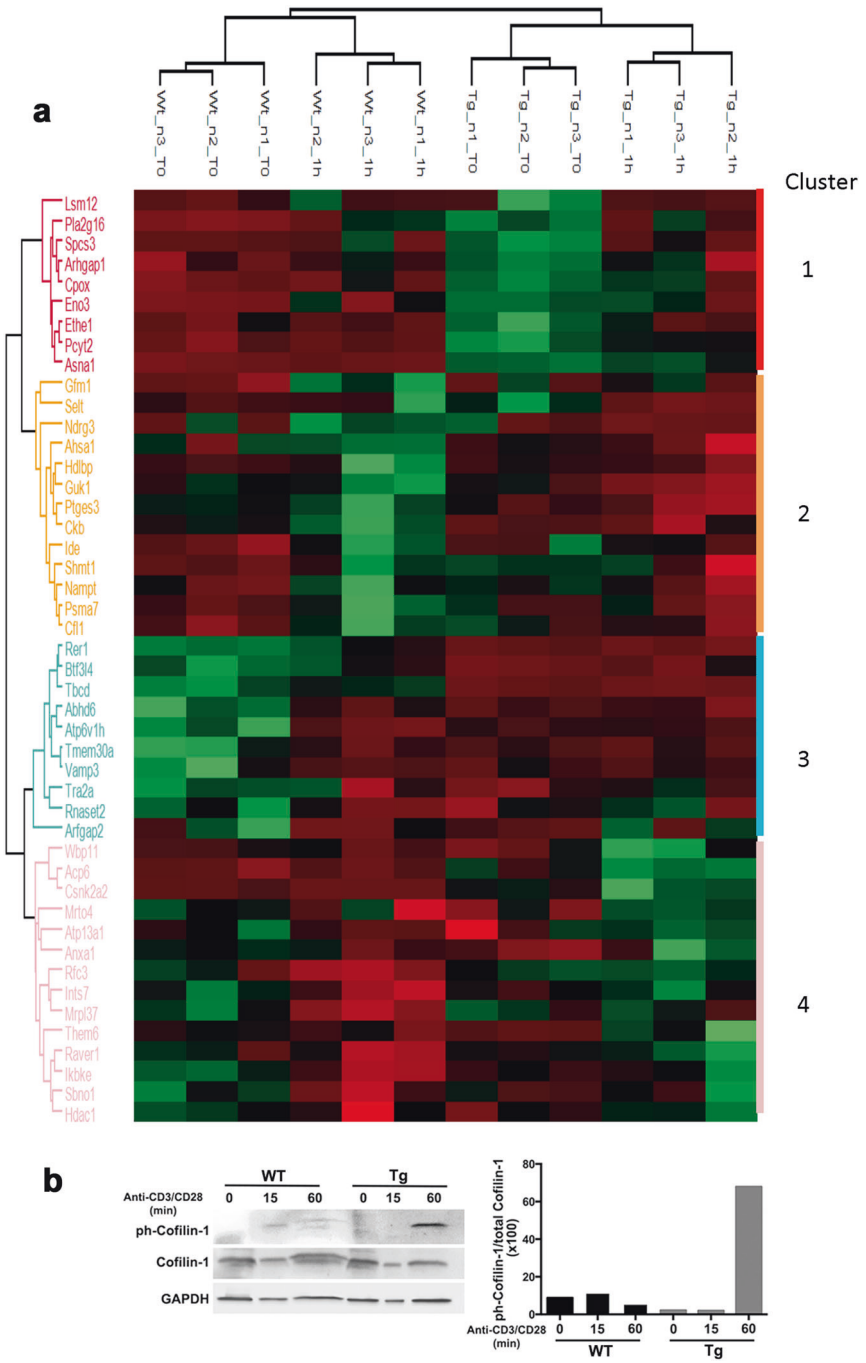

Fig. 9 Impact of CMIP expression and T cell activation on the total proteome. **a** Heat map showing 46 differentially expressed proteins in T cells obtained from transgenic and WT mice that were or were not subjected to 60 min of costimulation with anti-CD3/CD28 antibodies (1 μg/ml each). The column tree denotes mice grouped by hierarchical clustering. Rows correspond to 46 proteins whose differential expression was significant according to two-way ANOVA ($p < 0.01$) distributed into four clusters. Each cluster corresponds to proteins showing a similar pattern in variation depending on both parameters (CMIP expression and T cell activation). Proteins are labeled with their gene acronyms. **b** Phosphorylation/inactivation of Cofilin-1 in transgenic T cells. Western blot showing cofilin-1 in total extracts of transgenic and WT T cells isolated by negative immunoselection at reset (0 min) and after 15 or 60 min of costimulation with anti-CD3/CD28 antibodies (1 μg/ml each). Samples were analyzed with an anti-pSer3-Cofilin-1 antibody that recognizes the inactive form of cofilin-1 and an antibody recognizing the total Cofilin-1. GAPDH was used as a loading control. The right panel shows the inactive/total Cofilin-1 ratio according to densitometric analysis

dramatically increased in transgenic T cells at 60 min after stimulation compared to its levels in WT T cells (Fig. 9b). Likewise, Cofilin-1 was hyperphosphorylated in HEK cells overexpressing CMIP compared to its levels in cells transfected with a control vector (data not shown), suggesting a functional connection between CMIP overexpression and Cofilin-1 inactivation.

DISCUSSION

Little is known about the role of CMIP in vivo and the functional consequences of its overexpression in T cells, which led us to generate a transgenic mouse model in which CMIP was selectively induced in peripheral T cells. We show the following for the first time: (i) CMIP interferes with the early events of T cell signaling by

Table 1. Protein clusters differentially expressed between transgenic and wild-type T cells (see text for details)

Cluster	Two-way ANOVA p value Interaction	Protein names	Gene names
	0.0173924	ATPase Asna1	Asna1
	0.0346941	Beta-enolase	Eno3
	0.0382656	Oxygen-dependent coproporphyrinogen-III oxidase, mitochond	Cpox
	0.0198362	Rho GTPase-activating protein 1	Arhgap1
	0.00452375	HRAS-like suppressor 3	Pla2g16
	0.00564185	Ethanolamine-phosphate cytidylyltransferase	Pcyt2
	0.0447962	Protein LSM12 homolog	Lsm12
	0.00512036	Signal peptidase complex subunit 3	Spcs3
	0.0185284	Persulfide dioxygenase ETHE1, mitochondrial	Ethe1
	0.0120071	Cofilin-1	Cfl1
	0.029132	Serine hydroxymethyltransferase, cytosolic	Shmt1
	0.0207588	Selenoprotein T	Selt
	0.0308264	Creatine kinase B-type	Ckb
	0.00710747	Guanylate kinase	Guk1
	0.0328974	Activator of 90 kDa heat shock protein ATPase homolog 1	Ahsa1
	0.0272387	Elongation factor G, mitochondrial	Gfm1
	0.0336463	Vigilin	Hdlbp
	0.0136928	Nicotinamide phosphoribosyltransferase	Nampt
	0.0350412	Insulin-degrading enzyme	Ide
	0.037093	Protein NDRG3	Ndrg3
	0.0210732	Prostaglandin E synthase 3	Ptges3
	0.0274492	Proteasome subunit alpha type-7	Psma7
	0.0342864	Histone deacetylase 1	Hdac1
	0.0202517	Casein kinase II subunit alpha	Csnk2a2
	0.0197042	Annexin A1	Anxa1
	0.0223226	Protein strawberry notch homolog 1	Sbno1
	0.00719299	Integrator complex subunit 7	Ints7
	0.0246058	Protein THEM6	Them6
	0.0237745	Lysophosphatidic acid phosphatase type 6	Acp6
	0.0187061	Replication factor C subunit 3	Rfc3
	0.0401453	39S ribosomal protein L37, mitochondrial	Mrpl37
	0.0486016	WW domain-binding protein 11	Wbp11
	0.0214666	Ribonucleoprotein PTB-binding 1	Raver1
	0.0289481	mRNA turnover protein 4 homolog	Mrto4
	0.0357342	Manganese-transporting ATPase 13A1	Atp13a1
	0.0059116	Inhibitor of nuclear factor kappa-B kinase subunit epsilon	Ikbke
	0.0410545	Vesicle-associated membrane protein 3	Vamp3
	0.0413756	Transformer-2 protein homolog alpha	Tra2a
	0.000649362	V-type proton ATPase subunit H	Atp6v1h
	0.0444177	Tubulin-specific chaperone D	Tbcd
	0.00897285	Monoacylglycerol lipase ABHD6	Abhd6
	0.0217469	Cell cycle control protein 50A	Tmem30a
	0.0403846	ADP-ribosylation factor GTPase-activating protein 2	Arfgap2
	0.0478009	Ribonuclease T2	Rnaset2
	0.0380768	Transcription factor BTF3 homolog 4	Btf3l4
	0.0360256	Protein RER1	Rer1

inhibiting the activation of Src kinases (Fyn and Lck) and Zap-70 and their localization to LRs; (ii) CMIP inhibits LR clustering, which is required for immunological synapse formation; and (iii) transgenic T cells in which CMIP is selectively induced exhibit a lower proliferative capacity and are less prone to produce cytokines after their stimulation than WT T cells. In addition, the transgenic mice displayed a higher percentage of T cells with a naïve T cell phenotype and a lower reactivity to CD3/CD28 stimulation than WT

mice, as reflected by a decrease in IL-2 production. The inability to produce sufficient IL-2 may explain why transgenic T cells fail to proliferate and to differentiate like WT T cells. However, the addition of recombinant IL-2 to the culture medium restored their proliferative capacity. These results are consistent with previous data obtained from a randomized multicenter clinical trial that included cytokine and CMIP expression studies in the same patients at relapse and remission.[6] Indeed, we found that MCNS relapse is associated with the downregulation of IL2 and a concomitant increase in CMIP abundance. Altogether, these findings suggest that CMIP inhibits the differentiation of naïve T cells to effector cells and acts as a negative regulator of T cell signaling. IL-10 plays a key role in preventing inflammatory and autoimmune processes.[25] Given the contrasting effects of CMIP induction on cytokine production marked by the downregulation of IFNγ and IL4 and the increased production of IL-10, we postulate that increased Cmip abundance interferes with T cell differentiation into Th1 or Th2 cell subsets but may facilitate the development of regulatory T cell responses.

Although we focused on the study of early signaling events in T cells here, the finding that the Tg T cells were insensitive to PMA/ionomycin activation is unexpected because the recruitment of proximal signals is traditionally thought to be uncoupled from downstream effectors. Indeed, the inhibitory effects of Cmip seem to involve proximal events occurring in T cell signaling, as well as transcriptional machinery leading to cytokine synthesis. The fact that the PMA/ionomycin-mediated stimulation of IL-4 and IFNγ was sensitive to Cmip inhibition suggests two potential mechanisms that are not mutually exclusive. The first mechanism relies on the crossregulation of factors involved in early T cell proximal events and PKCθ. PKCθ has been shown to associate with CD28 in PMA-stimulated T cells and physically interact with ZAP70 in lipid rafts, leading to the activation of downstream signaling pathways and cytokine synthesis.[26] Moreover, PKCθ inhibits the suppressive function of regulatory T cells.[27] Determining whether Cmip can disrupt this regulatory loop requires additional investigation. The second mechanism implies the direct effect of Cmip as a repressor of NF-kB activity.[11,14] NF-kB binds to the CD28-responsive element in the *Il-2* promoter and acts as a potent transactivator.[28] Moreover, NF-kB can be activated by the stimulation of PKC by PMA.[29] The influence of Cmip on the transcriptional regulation of cytokines remains to be investigated.

The most proximal signaling events following T cell engagement involve the Src family tyrosine kinases Lck and Fyn. The abundance of the inactive Src kinases Fyn and Lck was significantly increased following the CD3/CD28-induced stimulation of transgenic T cells, whereas active Src kinase forms assessed by pY^{418}Src were reduced, suggesting that the early molecular events leading to the recruitment and activation of Src kinases in LRs are altered in the presence of CMIP. Activation of T cells by CD3/CD28 resulted in the polarization of LRs, which are enriched in Src kinases, GPI-linked proteins and adapter proteins that function together as signaling platforms. Because Lck is required for the tyrosine phosphorylation of CD28 and the recruitment of Zap70, its inactivation affects the early events of proximal signaling, which are critical for the migration of T cell receptors into LRs.[30] Our results suggest that Lck is maintained in its inactive conformation in transgenic T cells, preventing Zap 70 activation and LAT recruitment in LRs. We show here that T cell polarization, as visualized by CTxB staining, is inhibited after CD3/CD28 stimulation in transgenic T cells, while it is clearly observed in WT T cells. Collectively, these results suggest that CMIP inhibits proximal signaling and prevents the recruitment of LRs to the immunological synapse. These two observations—the defects in both the localization of proteins in LRs and LR clustering—are complementary. These processes can be linked, but the data provided by both approaches are independent. CTxB analysis cannot inform about the distribution of Src kinases in LRs, whereas LR isolation and WB cannot inform about raft clustering at the TCR. Altogether, the results of these approaches indicate the existence of an underlying mechanism involving CMIP that leads to LR disruption.

Our lipidomic analysis revealed ganglio-series glycosphingolipid synthesis to be the main metabolic pathway impacted by Cmip expression in a model cell line. This finding was consistent with the alterations in membrane raft signaling induced by Cmip expression in T cells. GM3, the precursor of GM1 and GM2, is the most abundant class of gangliosides in T cells,[31] where GM3 gangliosides seem to play a key role in activation and signal transduction and notably colocalize with the protein tyrosine kinase ZAP70.[32] Hence, the observed depletion of GM2 and GM3 cellular content and GM1 localization due to CMIP expression could be fundamental in the inhibition of immunological synapse formation suggested by our results.

T cell proximal signaling requires the integrity of LRs based on the following arguments: (1) GM3 is the main component of LRs, and the activation of $CD4^+$ T cells is severely compromised in G3-deficient mice, highlighting the functional relevance of LRs in T cell signaling.[33] (2) LR clustering occurs at the interface between T cell and antigen-presenting cell, forming the immunological synapse.[34,35] (3) The Src kinases Lck and Fyn, ZAP-70 kinase and adapter proteins, among others, are recruited to LRs.[36] Finally, (4) actin cytoskeleton rearrangement structurally regulates LR dynamics.[37] We have previously shown that CMIP interacts physically with Fyn and filamin A, so it may interfere with both LR and cytoskeleton dynamics.[13,38] Altogether, these data suggest that the negative regulatory role of CMIP is complex and affects early events in T cell signaling. However, the way in which CMIP inhibits LR dynamics by reducing GM3 and GM2 generation remains to be unveiled.

The importance of LRs in T cell activation lies in their ability to promote the efficient recruitment of membrane receptors and proximal protein partners by serving as a signaling platform and coordinate rearrangement of the actin cytoskeleton, which is required to enable sustained activation of the T cell response.[39] We sought to understand the impact of CMIP on these molecular events by differential proteomics and found four clusters of proteins that display significant differences in expression in transgenic T cells compared with WT T cells. We confirmed that cofilin-1, a major mediator of actin dynamics, is inactivated in transgenic T cells. T cell stimulation in the presence of cell-permeable cofilin peptide homologs has been shown to inhibit the interaction of cofilin with F-actin filaments, resulting in the impaired formation of the immune synapse, reduced production of T helper 1 (Th1) and Th2 cell cytokines, and reduced cell proliferation.[23]

CMIP is a new PH domain-containing and LRR domain-containing protein originally identified in T cells from patients with MCNS.[5] Several investigations carried out over the last decade have shed new light on the structural and functional characteristics of CMIP.[40] The recent observation that CMIP is overproduced in the tumor cell environment in patients who develop MCNS, even idiopathic MCNS, in the context of cancer raises intriguing questions and possibly implicates CMIP in the pathophysiological process of MCNS.[9] To date, CMIP has been found to interact with multiple partners, interfere with cytoskeletal dynamics, downregulate NF-kB activity and promote apoptosis.[38] Its involvement in different signaling pathways suggests that CMIP is present in multiple complexes that regulate the response to intracellular and membrane receptors. The current study adds new insight into CMIP function and suggests the negative regulatory role of CMIP in T cell signaling. Negative regulation is critical for the termination of immune responses, peripheral tolerance and the prevention of inflammation-induced tissue damage. Sustained activation of T lymphocytes resulting from a lack of feedback control can lead to autoimmune diseases, transplant rejection and

cancer. Conversely, excess negative regulation may impede appropriate T cell activation in response to pathogens and lead to chronic infection. In addition, the inability to engage appropriate T cell responses against tumoral neoantigens results in cellular proliferation and metastasis. Indeed, the induction of inhibitory molecules, such as CTLA-4 and PD-1, was found to be correlated with viral load,[41] and in cancer,[42] the blockade of these inhibitory molecules provides a clear survival benefit.[43] However, our results do not exclude a role for CMIP as a modulator of T cell activation and the immune response. Thus, a better understanding of the role of CMIP in the negative regulation of T cell signaling may open new therapeutic perspectives to manipulate the immune system.

MATERIALS AND METHODS

Patients

Ten adult patients were included after their informed consent was obtained. The diagnosis of MCNS was confirmed by renal biopsy before inclusion. All patients with relapse had proteinuria >3 gr/24 h and low serum albumin levels (<30 gr/l). Blood samples were obtained at the time of diagnosis before treatment. Remission samples were collected during periods of inactive disease defined by proteinuria <0.2 g/24 h without steroid treatment. Samples were obtained in the context of a clinical trial (Clinical trial.gouv identifier: NCT01197040) with the written consent of participants involved in this study.

Generation of CMIP transgenic mice

A transgenic mouse model was constructed with a targeting system based on the reconstitution of a functional X-linked hypoxanthine-guanine phosphoribosyltransferase (Hprt) locus as previously described.[38] The full-length coding sequence of human CMIP was inserted downstream of the distal Lck promoter, allowing CMIP expression in only peripheral T-lymphocytes.[18] The HPRT PCR product was amplified in WT and heterozygous transgenic female ($Tg^{+/-}$) mice but not in mice with reconstituted HPRT alleles, such as homozygous transgenic female ($Tg^{+/+}$) or hemizygous transgenic male (Tg+) mice. The CMIP and HPRT PCR products were 309 and 301 base pairs in size, respectively (Table S1).

The experimental procedures were approved by the National Ethics Committee (COMETH) under accreditation number 29/01/13-1.

Generation of conditional and inducible T cell-specific CMIP knockout mice

Details of the construction of $Cmip^{lox/lox}$ mice have been previously reported.[17] A triple transgenic mouse strain (CD2-rtTA/TetOn-Cre/$CMIP^{loxP/loxP}$) was generated by sequential crossing. We first crossed $Cmip^{lox/lox}$ mice with C.Cg-Tg(tetO-cre)1Jaw/J mice (strain N° 006244) that were purchased from Jackson laboratory (Bar Harbor, ME USA). Then, the homozygous double transgenic TetO-Cre/CmipLox mice were crossed with Tg(CD2-rtTA)CRza mice (a generous gift of R Zamoyska, MRC, London, UK). The offspring were subsequently intercrossed until mice homozygous for the three genes were obtained.

Flow cytometry analysis

Splenocytes were incubated for 10 min at room temperature (RT) with TruStain fcX™ (BioLegend) and then stained with anti-mouse fluorochrome-conjugated mAbs against CD4, CD8, CD44, and CD62L for 20 min at RT. The CD4-FITC and CD62L-PE antibodies were purchased from Miltenyi Biotec, and the CD8-APC and CD44-Pecy7 antibodies were purchased from eBiosciences (Table S2A). Splenocytes were then fixed for 7 min with 4% paraformaldehyde and analyzed by flow cytometry on a FACS CyAn ADP analyzer (Beckman Coulter) using FlowJo software (Tree Star, San Carlos, CA, USA).

T cell isolation

Spleens were harvested, gently minced with a scalpel and passed through a 40 µM nylon mesh filter. Mononuclear cells were isolated with a Ficoll® 400 (Eurobio) density gradient. Purified T cells were isolated by negative selection using a Pan T Cell isolation kit (Miltenyi Biotec GmbH, Germany).

Ex vivo T cell stimulation

Before stimulation, T cells were systematically synchronized at the G1 phase of the cell cycle by serum starvation in 2% fetal calf serum (FCS) for 6 h. Synchronized T cells were then activated for the indicated times with soluble anti-CD3 and anti-CD28 antibodies (eBiosciences, San Diego, CA, USA) at 1 µg/ml in RPMI complete medium supplemented with 10% FCS. In another set of experiments, T cells were activated with phorbol 12-myristate 13-acetate (PMA, 50 ng/ml) and ionomycin (0.5 µg/ml) for the indicated times in similar culture conditions.

Western blot analysis

All primary antibodies used in this study are referenced in Table S2B. Western blotting was performed as previously described.[38]

Quantification of transcripts by reverse transcription and real-time quantitative PCR (RT-qPCR)

Total RNA was extracted and purified using an RNeasy kit (Qiagen, Inc., Germantown, USA) following the supplier's protocol. The sequences of the primers used are listed in Table S1. RT-qPCR was performed as previously described.[7] All RT-qPCRs were performed in duplicate, and expression levels were normalized to 18S rRNA expression. Cycle threshold (CT) values were calculated using the relative quantification method (Applied Biosystems). Relative copy numbers were calculated by determining the difference in the CT between the target and control probes ($\Delta CT = CT_{gene\ of\ interest} - CT_{18S}$). Samples amplified with cycle thresholds greater than 32 were excluded from the analyses. The fold-change in mRNA induction relative to that in unstimulated cells was evaluated by the $2^{-\Delta\Delta CT}$ method.

T cell proliferation assay

T cell proliferation was determined by the extent of carboxyfluorescein diacetate succinimidyl ester (CFSE) dye dispersion in the culture at day 5 in the presence of soluble anti-CD3/anti-CD28 antibodies (1 µg/ml each). For CFSE labeling, synchronized T cells were resuspended at 10^7 cells/ml in PBS containing 1 µM CFSE (eBioscience) and incubated for 10 min at RT. The labeling reaction was terminated by the addition of 3 volumes of cold PBS. Then, the cells were washed three times, resuspended in RPMI complete medium supplemented with 10% FCS at 10^7 cells/ml in the presence of soluble anti-CD3/CD28 antibodies (1 µg/ml) with or without IL-2 (30 UI/ml), and incubated for five days. The incorporation of CFSE was measured by flow cytometry.

Immunocytochemistry

T cells were plated at 10^4 cells/slide using a cytospin centrifuge, fixed in 4% PFA for 10 min at RT, and then permeabilized by incubation with 0.3% Triton X-100 for 10 min. Endogenous biotin and avidin were blocked using an Avidin-Biotin Blocking kit (Vector Laboratories). Membranous ganglioside GM1 was visualized by direct incubation with Alexa Fluor555-conjugated cholera toxin subunit B (Molecular Probes, 8 µg/ml in PBS, 50 µl/slide) for 25 min at RT and washed (3 × 5 min) before being covered with Vectashield mounting medium containing DAPI (4′,6-diamidino-2-phenylindole) (Vector Laboratories), following which the slides were viewed under a fluorescence microscope (Zeiss, Germany)

with the appropriate filters. A rabbit polyclonal antibody developed in our laboratory was used (1:1000 dilution) to visualize CMIP. An anti-CMIP antibody recognizing both human and mouse CMIP has been previously described.[17] To ensure the specificity of each signal, IgG isotype control antibody (Cell Signaling) was used instead of primary antibody in control samples.

Confocal and video microscopy

All fluorescent images were collected on a Zeiss LSM510 confocal microscope. For live imaging experiments, synchronized T cells were stained with AF555-CTB (Molecular Probes, 8 µg/ml), seeded onto 8-well ibiTreat µ-Slides (Ibidi, Biovalley S.A., France), and then stimulated with CD3-coated beads (human Dynabeads CD3, Invitrogen) and soluble anti-CD28 (1 µg/ml, eBiosciences) at a 2:1 ratio. One image was collected every 15 s. Samples were maintained at 37 °C.

Lipid raft preparation

Lipid raft microdomains were obtained by a detergent-free method based on the method described by McDonald and Pike.[44] Between 15 and 30 million cells per sample were washed twice in cold PBS, resuspended in 800 µl of MBS/Na_2CO_3 buffer (25 mM MES, 150 mM NaCl, 250 mM Na_2CO_3, pH 6; supplemented with 1 mM PMSF and phosphatase and protease inhibitor cocktails) and lysed by 20 passages through a 21 G needle, followed by sonication 3 times for 60 s in a Vibra-Cell 75022 sonicator. The homogenate was mixed with two volumes of 60% OptiPrep™ (Axis Shield) in a final volume of 2 ml containing 40% OptiPrep™. A three-step discontinuous density gradient was made by adding 2 ml of 30% OptiPrep™ in MBS/Na_2CO_3 buffer and 1 ml of 5% OptiPrep™ sequentially to the top of the homogenate. The mixture was spun in a TL-100 rotor at 268,000×*g* for 2 h in an Optima MAX-XP ultracentrifuge (Beckman Coulter). After spinning, 8 fractions of 600 µl each and the pellet were recovered from top to bottom. For most studies, fractions 2, 3, and 4 and fractions 6, 7, and 8 were pooled separately and labeled as R (rafts) and NR (nonrafts), respectively. These pools were characterized using the established lipid and protein raft markers Flotillin-1 and cholesterol, respectively. For Western blot studies, proteins from the R and NR fractions were precipitated by the addition of 10% trichloroacetic acid (final concentration), incubation overnight at −20 °C and three washes in cold ethanol. The resultant dry protein pellets were solubilized in equal volumes of 5× Laemmli buffer and stored at −80 °C until use.

High-performance thin-layer chromatography (HPTLC)

Cholesterol levels were evaluated by thin layer chromatography as previously described.[45] Briefly, the R and NR fractions were subjected to organic extraction by the addition of 6 volumes of chloroform/methanol (2:1, v/v) and thorough vortexing, followed by centrifugation at 3000 × *g* for 5 min. The organic lower phase was recovered and evaporated to dryness under a nitrogen stream. The dry lipid film was resuspended in 20 µl of chloroform/methanol (1:1, v/v). Five microliters of each sample was spotted on a Partisil HPK 60 Å silica HPTLC plate (Whatman) along with 3 µg of cholesterol standard, predeveloped in chloroform/methanol (1:1, v/v) and developed in chloroform/acetone (95:5, v/v). Bands were detected by dipping the plate into a solution of 626.6 mM CuSO4 and 8% H_3PO_4 followed by charring at 160 °C.

Lipid extraction, untargeted lipidomics and analysis of ganglioside metabolism

Untargeted lipidomics was optimized in immortalized mouse podocytes stably transfected with a vector carrying the coding sequence of CMIP or an empty vector as a control. The cell line characteristics and culture conditions have been described before.[38] Five million cells per sample were subjected to organic extraction. Lipids were extracted by adding methanol to dry cell pellets and centrifuging them at 10,000×*g* for 10 min at 4 °C. The supernatant was then subjected to liquid chromatography-mass spectrometry (LC-MS) analysis using an ionKey/MS system with an Acquity UPLC M-Class system, ionKey source, and an iKey CSH C18 (130 Å, 1.7 µm particle size, 150 µm × 100 mm) column (Waters) coupled to a Synapt G2-Si mass spectrometer (Waters). Analyses were conducted in both positive and negative electrospray ionization mode using data-independent acquisition. The capillary voltage was 2.8 kV, and the source temperature was 110 °C. Injections of 0.5 µl were carried out in partial loop mode, the column temperature was 55 °C, and the flow rate was 3 µl/min. Mobile phase A consisted of acetonitrile/water (60:40) with 10 mM ammonium formate + 0.1% formic acid. Mobile phase B consisted of 2-propanol/acetonitrile (90:10) with 10 mM ammonium formate + 0.1% formic acid. The gradient was programmed as follows: 0.0−2.0 min, from 40 to 43% B; 2.0−2.1 min, from 43 to 50% B; 2.1−12.0 min, from 50 to 99% B; 12.0−12.1 min, from 99 to 40% B; and 12.1−14.0 min, 40% B.

Data processing and analysis were conducted using Progenesis QI Informatics (Nonlinear Dynamics, Newcastle, UK) and MetaboAnalyst 3.0 software.[46] Each UPLC-MS run was imported as an ion intensity map that included m/z and retention time. These ion maps were then aligned along the retention time direction. From the aligned runs, an aggregate run representing the compounds in all samples was used for peak picking. This aggregate run was then compared with all runs so the same ions were detected in every run. Isotope and adduct deconvolution was applied to reduce the number of features detected. Data were normalized according to total ion intensity. Lipids of interest were filtered for further identification using ANOVA $p < 0.001$ and a fold-change > 5.

Lipids were identified by database searches against their accurate masses using the publicly available databases Lipid Metabolites and Pathways Strategy (LIPID MAPS) and Human Metabolome database (HMDB) and by fragmentation patterns and retention times when available. Pathway analysis consisting of enrichment analysis and pathway topological analysis was conducted using Metabolomics Pathway Analysis (MetPA) within MetaboAnalyst.[47] Additional pathway overrepresentation analyses were conducted using Integrated Molecular Pathway Level Analysis (IMPaLA).[48]

Proteomic analysis of T cells isolated from WT and transgenic mice *MS/MS protein identification and quantification*. Cells were lysed in 2% SDS and boiled at 95 °C for 5 min. Filter-Aided Sample Preparation (FASP) was used for protein digestion. Briefly, cell lysates were treated with 100 mM DTT for 30 min at 60 °C, mixed with 8 M urea buffer, loaded on Microcon 30 kDa centrifugal filters (Millipore) and alkylated with 50 mM iodoacetamide. The filters were washed twice with 8 M urea and twice with 50 mM ammonium bicarbonate. Following overnight trypsin digestion at 37 °C, the samples were vacuum dried and resuspended in 10% acetonitrile and 0.1% formic acid for LC-MS/MS. For each run, 1 µg of sample was analyzed by a nanoRSLC-Q Exactive PLUS MS (Dionex RSLC Ultimate 3000, Thermo Scientific, Waltham, MA, USA). Peptides were separated on a reversed-phase liquid chromatographic column (Pepmap C18, Dionex). The solvents used during chromatography were (A) 0.1% formic acid in water and (B) 80% acetonitrile and 0.08% formic acid. Peptides were eluted from the column with the following gradient: 5 to 40% B (120 min) and 40 to 80% (7 min). After 127 min, the gradient returned to 5% to re-equilibrate the column for 20 min before the next injection. Two blanks and two long 75 min step gradients were run between technical and biological triplicate samples to prevent sample carryover. Peptides eluting from the column were analyzed by data-dependent MS/MS using the Top 10 acquisition method. Briefly, the instrument settings were as follows. The resolution was set to 70,000 for MS scans and 17,500 for

data-dependent MS/MS scans to increase speed. The MS AGC target was set to 3106 counts, while the MS/MS AGC target was set to 5104. The MS scan range was from 400 to 2000 *m/z*. MS and MS/MS scans were recorded in profile mode. Dynamic exclusion was set to a 30 s duration. Three replicates of each sample were analyzed by nanoLC/MS/MS.

Data processing following LC-MS/MS acquisition. The raw MS data were processed with MaxQuant software version 1.5.2.8, and the Andromeda search engine was used to search the raw MS data against the *Mus musculus* subset of the UniProtKB/SwissProt database (release 2015-03-04, 16704 sequences). To search parent mass and fragment ions, we used search mass deviations of 4.5 ppm and 20 ppm, respectively. The minimum peptide length was set to 7 amino acids, and strict specificity for trypsin cleavage allowing up to two missed cleavage sites was required. Carbamidomethylation (Cys) was set as a fixed modification, whereas oxidation (Met) and N-term acetylation were set as variable modifications. The false discovery rates (FDRs) at the protein and peptide levels were set to 1%. Scores were calculated in MaxQuant as described previously.[49] The reverse and common contaminant hits were removed from the MaxQuant output. Proteins were quantified according to the MaxQuant label-free algorithm using LFQ intensities;[22,23] protein quantification was obtained using at least 2 peptides per protein. Statistical and bioinformatic analyses, including heatmaps, profile plots and clustering, were performed with Perseus software (version 1.5.0.31), which is freely available at www.perseus-framework.org. For each protein, LFQ values corresponded to the average LFQ from three technical triplicates. We filtered the data to keep only proteins with at least 5 valid values out of 12. Next, the data were input to fill missing data points by creating a Gaussian distribution of random numbers with a standard deviation of 33% relative to the standard deviation of the measured values and a 1.8 standard deviation downshift of the mean to simulate the distribution of low signal values. For statistical comparison of 2 pairs of groups (Lck vs. Balb/c mice and stimulated vs. nonstimulated mice), two-way ANOVA was performed ($p < 0.05$). Hierarchical clustering of proteins whose expression levels were significantly different between Lck vs. Balb/C mice and stimulated vs. nonstimulated mice and proteins exhibiting a significant interaction between the two pairs of groups were performed in Perseus on logarithmized LFQ intensities after z-score normalization of the data using Euclidean distances.

Statistical analysis

Data were analyzed with Prism Software for Macintosh (GraphPad Software, Inc., USA). Differences between the two different groups was determined by using Student's *t*-test. *P* values of less than 0.05 indicated statistical significance.

ACKNOWLEDGEMENTS

We are grateful to Prof. Rose Zamoyska (Medical Research Council, London, United Kingdom) for providing us with the Tg(CD2-rtTA) CRza mouse model. This work was supported in part by a grant from the French Kidney Foundation. J.O., P.V., and K.S. were supported by grants from the Ministry of Research.

AUTHOR CONTRIBUTIONS

J.O., K.S., C.C., P.V., B.S., E.C., C.H., V.F., A.P., G.A. and I.C.G. performed the experiments. M.O., V.A. and D.S. wrote the paper. D.S. and M.O. supervised the project. All authors discussed the results and participated in writing the paper.

ADDITIONAL INFORMATION

The online version of this article (https://doi.org/10.1038/s41423-019-0266-5) contains supplementary material.

Competing interests: The authors declare no competing interests.

REFERENCES

1. Brubaker, S. W., Bonham, K. S., Zanoni, I. & Kagan, J. C. Innate immune pattern recognition: a cell biological perspective. *Annu. Rev. Immunol.* **33**, 257–290 (2015).
2. Chakraborty, A. K. & Weiss, A. Insights into the initiation of TCR signaling. *Nat. Immunol.* **15**, 798–807 (2014).
3. Viola, A. & Gupta, N. Tether and trap: regulation of membrane-raft dynamics by actin-binding proteins. *Nat. Rev. Immunol.* **7**, 889–896 (2007).
4. Brownlie, R. J. & Zamoyska, R. T cell receptor signalling networks: branched, diversified and bounded. *Nat. Rev. Immunol.* **13**, 257–269 (2013).
5. Sahali, D. et al. A novel approach to investigation of the pathogenesis of active minimal- change nephrotic syndrome using subtracted cDNA library screening. *J. Am. Soc. Nephrol.* **13**, 1238–1247 (2002).
6. Boumediene, A. et al. NEPHRUTIX: a randomized, double-blind, placebo vs Rituximab-controlled trial assessing T-cell subset changes in Minimal Change Nephrotic Syndrome. *J. Autoimmun*. **88**, 91–102 (2018).
7. Sendeyo, K. et al. Upregulation of c-mip is closely related to podocyte dysfunction in membranous nephropathy. *Kidney Int.* **83**, 414–425 (2013).
8. Bouachi, K. et al. Expression of CMIP in podocytes is restricted to specific classes of lupus nephritis. *PLoS ONE* **13**, e0207066 (2018).
9. Audard, V. et al. Occurrence of minimal change nephrotic syndrome in classical Hodgkin lymphoma is closely related to the induction of c-mip in Hodgkin-Reed Sternberg cells and podocytes. *Blood* **115**, 3756–3762 (2010).
10. Bouatou, Y. et al. Nephrotic syndrome in small cell lung cancer and induction of C-Mip in podocytes. *Am. J. Kidney Dis*. 2017;69:477–480.
11. Kamal, M. et al. C-mip interacts physically with RelA and inhibits nuclear factor kappa B activity. *Mol. Immunol.* **46**, 991–998 (2009).
12. Kamal, M. et al. C-mip interacts with the p85 subunit of PI3 kinase and exerts a dual effect on ERK signaling via the recruitment of Dip1 and DAP kinase. *FEBS Lett.* **584**, 500–506 (2010).
13. Grimbert, P. et al. The Filamin-A is a partner of Tc-mip, a new adapter protein involved in c-maf-dependent Th2 signaling pathway. *Mol. Immunol.* **40**, 1257–1261 (2004).
14. Izzedine, H. et al. Expression patterns of RelA and c-mip are associated with different glomerular diseases following anti-VEGF therapy. *Kidney Int.* **85**, 457–470 (2014).
15. Ory, V. et al. c-mip down-regulates NF-kappaB activity and promotes apoptosis in podocytes. *Am. J. Pathol.* **180**, 2284–2292 (2012).
16. Izzedine, H. et al. Kidney diseases associated with anti-vascular endothelial growth factor (VEGF): an 8-year observational study at a single center. *Medicine* **93**, 333–339 (2014).
17. Moktefi, A. et al. Repression of CMIP transcription by WT1 is relevant to podocyte health. *Kidney Int.* **90**, 1298–1311 (2016).
18. Nakao, A. et al. Blockade of transforming growth factor beta/Smad signaling in T cells by overexpression of Smad7 enhances antigen-induced airway inflammation and airway reactivity. *J. Exp. Med.* **192**, 151–158 (2000).
19. Ballarin-Gonzalez, B. et al. Protection and systemic translocation of siRNA following oral administration of Chitosan/siRNA nanoparticles. *Mol. Ther. Nucleic Acids* **2**, e76 (2013).
20. Gao, S. et al. The effect of chemical modification and nanoparticle formulation on stability and biodistribution of siRNA in mice. *Mol. Ther.* **17**, 1225–1233 (2009).
21. Malissen, B. & Bongrand, P. Early T cell activation: integrating biochemical, structural, and biophysical cues. *Annu Rev. Immunol.* **33**, 539–561 (2015).
22. Zeng, P., Xu, Y., Zeng, C., Ren, H. & Peng, M. Chitosan-modified poly(D,L-lactide-co-glycolide) nanospheres for plasmid DNA delivery and HBV gene-silencing. *Int J. Pharm.* **415**, 259–266 (2011).
23. Eibert, S. M. et al. Cofilin peptide homologs interfere with immunological synapse formation and T cell activation. *Proc. Natl Acad. Sci. USA* **101**, 1957–1962 (2004).
24. Yu, L. et al. cMaf inducing protein inhibits cofilin1 activity and alters podocyte cytoskeleton organization. *Mol. Med. Rep.* **16**, 4955–4963 (2017).
25. Saraiva, M. & O'Garra, A. The regulation of IL-10 production by immune cells. *Nat. Rev. Immunol.* **10**, 170–181 (2010).
26. Xie, J. et al. Phosphotyrosine-dependent interaction between the kinases PKCtheta and Zap70 promotes proximal TCR signaling. *Sci. Signal.* 2019;12: eaar3349.
27. Zanin-Zhorov, A. et al. Protein kinase C-theta mediates negative feedback on regulatory T cell function. *Science* **328**, 372–376 (2010).
28. Ghosh, P., Tan, T. H., Rice, N. R., Sica, A. & Young, H. A. The interleukin 2 CD28-responsive complex contains at least three members of the NF kappa B family: c-Rel, p50, and p65. *Proc. Natl Acad. Sci. USA* **90**, 1696–1700 (1993).

29. Bomsztyk, K. et al. Evidence that interleukin-1 and phorbol esters activate NF-kappa B by different pathways: role of protein kinase C. *Cell Regul.* **2**, 329–335 (1991).
30. Zamoyska, R. et al. The influence of the src-family kinases, Lck and Fyn, on T cell differentiation, survival and activation. *Immunol. Rev.* **191**, 107–118 (2003).
31. Tuosto, L. et al. Organization of plasma membrane functional rafts upon T cell activation. *Eur. J. Immunol.* **31**, 345–349 (2001).
32. Garofalo, T. et al. Association of GM3 with Zap-70 induced by T cell activation in plasma membrane microdomains: GM3 as a marker of microdomains in human lymphocytes. *J. Biol. Chem.* **277**, 11233–11238 (2002).
33. Nagafuku, M. et al. CD4 and CD8 T cells require different membrane gangliosides for activation. *Proc. Natl Acad. Sci. USA* **109**, E336–E342 (2012).
34. Dykstra, M., Cherukuri, A., Sohn, H. W., Tzeng, S. J. & Pierce, S. K. Location is everything: lipid rafts and immune cell signaling. *Annu. Rev. Immunol.* **21**, 457–481 (2003).
35. Davis, D. M. & Dustin, M. L. What is the importance of the immunological synapse? *Trends Immunol.* **25**, 323–327 (2004).
36. Zumerle, S., Molon, B. & Viola, A. Membrane rafts in T cell activation: a spotlight on CD28 costimulation. *Front. Immunol.* **8**, 1467 (2017).
37. Ballek, O. et al. TCR triggering induces the formation of Lck-RACK1-Actinin-1 multiprotein network affecting Lck redistribution. *Front. Immunol.* **7**, 449 (2016).
38. Zhang, S. Y. et al. c-mip impairs podocyte proximal signaling and induces heavy proteinuria. *Sci. Signal.* **3**, ra39 (2010).
39. Varshney, P., Yadav, V. & Saini, N. Lipid rafts in immune signalling: current progress and future perspective. *Immunology* **149**, 13–24 (2016).
40. Sahali, D. et al. Immunopathogenesis of idiopathic nephrotic syndrome with relapse. *Semin. Immunopathol.* **36**, 421–429 (2014).
41. Kassu, A. et al. Regulation of virus-specific CD4+ T cell function by multiple costimulatory receptors during chronic HIV infection. *J. Immunol.* **185**, 3007–3018 (2010).
42. Hodi, F. S. et al. Biologic activity of cytotoxic T lymphocyte-associated antigen 4 antibody blockade in previously vaccinated metastatic melanoma and ovarian carcinoma patients. *Proc. Natl Acad. Sci. USA* **100**, 4712–4717 (2003).
43. Velu, V. et al. Enhancing SIV-specific immunity in vivo by PD-1 blockade. *Nature* **458**, 206–210 (2009).
44. Macdonald, J. L. & Pike, L. J. A simplified method for the preparation of detergent-free lipid rafts. *J. Lipid Res.* **46**, 1061–1067 (2005).
45. Bourderioux, M. et al. A new workflow for proteomic analysis of urinary exosomes and assessment in cystinuria patients. *J. Proteome Res.* **14**, 567–577 (2015).
46. Xia, J., Mandal, R., Sinelnikov, I. V., Broadhurst, D. & Wishart, D. S. MetaboAnalyst 2.0–a comprehensive server for metabolomic data analysis. *Nucleic Acids Res.* **40** (Web Server issue), W127–W133 (2012).
47. Li, F. et al. MPINet: metabolite pathway identification via coupling of global metabolite network structure and metabolomic profile. *BioMed. Res. Int.* 2014;2014:325697.
48. Cavill, R. et al. Consensus-phenotype integration of transcriptomic and metabolomic data implies a role for metabolism in the chemosensitivity of tumour cells. *PLoS Comput. Biol.* **7**, e1001113 (2011).
49. Cox, J. & Mann, M. MaxQuant enables high peptide identification rates, individualized p.p.b.-range mass accuracies and proteome-wide protein quantification. *Nat. Biotechnol.* **26**, 1367–1372 (2008).